Eddy-Current Field Analysis in Laminated Iron Cores Using Multi-Scale Model Order Reduction

Hamed Eskandari[1], Johan Gyselinck[2], and Tetsuji Matsuo[1]
[1]Graduate School of Engineering, Kyoto University, Kyoto, 615-8510 Japan
[2] Universite Libre de Bruxelles (ULB), Department of Electrical Engineering, Brussels B-1050, Belgium

This paper develops a multi-scale Model Order Reduction (MOR) method including both material and machine scale MOR. The material-scale MOR homogenizes the eddy-current (EC) field in laminated cores using the Legendre expansion of magnetic induction along the stacking direction within each steel sheet. The machine-scale MOR represents the EC field in electromagnetic devices with their equivalent Cauer Ladder Network (CLN). The former MOR is built into the latter by applying the CLN procedure to the homogenized EC field equation.

Index Terms—**Cauer Ladder Network, Eddy-Current, Laminated Core, Model Order Reduction, Multi-Scale.**

I. Introduction

ELECTROMAGNETIC drive systems require accurate and computationally cheap mathematical models for the design and control of their electrical equipment. These models are expected to cover all the complexities including the moving parts, magnetic nonlinearities and micro-structural properties over a wide range of frequencies. Analytically, Finite Element (FE) models, meet all these requirements, however, in practice its prohibitively large systems of equations makes them ineffective, less favorable and sometimes impossible to be used. This is where MOR comes into play by simplifying the large and complex systems of equations without loosing much accuracy [1], [2].

In magneto-quasistatic field analysis, variety of MOR methods are proposed which can be categorized into different groups. Here we would like to classify them as ”Machine-Scale” and ”Material-Scale” MORs. The former focuses on efficient electromagnetic field calculation over the whole machine on macroscopic scale; while the latter deals with the homogenization and expressing the components of electromagnetic equipment with fine structures, such as laminated steel sheets [3], [4] or windings [5], [6], on microscopic scale. This research aims to develop a multi-scale MOR, integrating the machine-scale and material-scale MOR into a single methodology.

Regarding the material-scale MORs, the simplest one is to consider the stacked laminated-core as a nonconducting nonhysteretic homogenous material and estimating the iron losses a posteriori. However, more advanced homogenizations have been developed to avoid the FE division along the stacking direction. Fig. 1 (a) illustrates how the material-scale MOR approximates a stacked laminated-core (left) into a homogenized bulk material (right); see e.g. [3] for a homogenization method that considers eddy currents and skin effect in laminated stacks using the Legendre polynomials.

Corresponding author: H. Eskandari (email: hamed.eskandari.28x@st.kyoto-u.ac.jp).

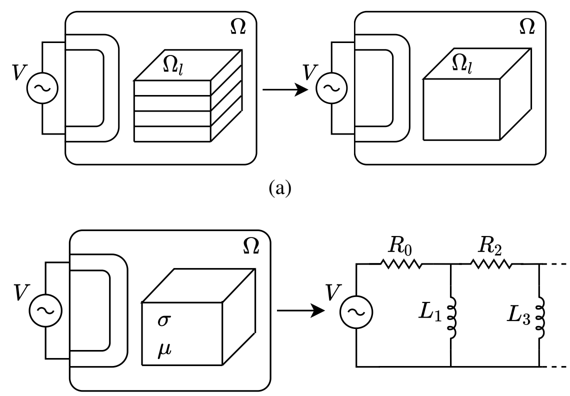

Fig. 1. (a) homogenization method as a material-scale MOR and (b) CLN method as a machine-scale MOR.

In this paper, among machine-scale MOR methods, the CLN method is chosen as one of the newly established MOR techniques, possessing clear physical interpretation, accuracy, and efficiency [7], [8], [10]. As it is shown in Fig. 1 (b), the CLN method finds the equivalent circuit network (right) for any linear domain governed by magneto-quasistic field (left).

The homogenization method in [3] has intrinsic compatibility with the CLN concept, which makes it a suitable choice to be incorporated with CLN method [9]. The main contribution of this paper is presenting a multi-scale MOR as a combination of the CLN method (machine-scale MOR) and Legendre polynomial based homogenization of laminated sheets (material-scale MOR).

II. Summary On The MORs

For the ease of comprehension and implementation, the mathematical terms are expressed in their matrix forms in FE context. When analyzing the magneto-quasistatic using the FE, the domain Ω is discretized via FE mesh encompassing m edges and n facets. The magnetic vector potential $\boldsymbol{A}$, electric field $\boldsymbol{E}$, and the magnetic flux density $\boldsymbol{B}$ are approximated by basis vector functions for the edge elements $\boldsymbol{w}_i^1$, and the facet elements $\boldsymbol{w}_j^2$ as

Algorithm 1 CLN Procedure

$\boldsymbol{a}_{-1} = 0$
$1/R_0 = \boldsymbol{e}_0^T \boldsymbol{\sigma} \boldsymbol{e}_0$
for $n = 0$ **to** $n = \#stages$ **do**
  $solve : \boldsymbol{K}\tilde{\boldsymbol{a}}_{2n+1} = R_{2n}\boldsymbol{\sigma}\boldsymbol{e}_{2n}$
  $\boldsymbol{a}_{2n+1} = \tilde{\boldsymbol{a}}_{2n+1} + \boldsymbol{a}_{2n-1}$
  $L_{2n+1} = \boldsymbol{a}_{2n+1}^T \boldsymbol{K} \boldsymbol{a}_{2n+1}$
  $\boldsymbol{e}_{2n+2} = \boldsymbol{e}_{2n} - L_{2n+1}^{-1}\boldsymbol{a}_{2n+1}$
  $1/R_{2n+2} = \boldsymbol{e}_{2n+2}^T \boldsymbol{\sigma} \boldsymbol{e}_{2n+2}$
end for

$$\boldsymbol{A} = \sum_i a_i \boldsymbol{w}_i^1, \quad \boldsymbol{E} = \sum_i e_i \boldsymbol{w}_i^1, \quad \boldsymbol{B} = \sum_j b_j \boldsymbol{w}_j^2, \tag{1}$$

where a_i and e_i are the line integrals of $\boldsymbol{A}$ and $\boldsymbol{E}$ over the edge i, and b_j the surface integral of $\boldsymbol{B}$ on the facet j [11]. Thus, $\boldsymbol{A}$ and $\boldsymbol{B}$ are expressed by column vectors with m and n entities, respectively

$$\boldsymbol{a} = [a_1, a_2, \ldots, a_m]^T, \ \boldsymbol{b} = [b_1, b_2, \ldots, b_n]^T. \tag{2}$$

The curl operator is equivalent to an $n \times m$ matrix $\boldsymbol{C}$, known as edge-face incident matrix (i.e., $\boldsymbol{B} = \boldsymbol{\nabla} \times \boldsymbol{A}$ is equivalent to $\boldsymbol{b} = \boldsymbol{C}\boldsymbol{a}$).

The quasi-static EC field equation in a linear region with magnetic permeability μ and electric conductivity σ leads

$$\boldsymbol{C}^T \boldsymbol{h} = \boldsymbol{C}^T \boldsymbol{\nu} \boldsymbol{C} \boldsymbol{a} = \boldsymbol{\sigma}\boldsymbol{e} + \boldsymbol{j}_0, \tag{3}$$
$$\boldsymbol{C}\boldsymbol{e} = -\partial_t \boldsymbol{b} = -\partial_t \boldsymbol{C}\boldsymbol{a}, \tag{4}$$

where $\boldsymbol{h}$ and $\boldsymbol{j}_0$ are discretized magnetic field strength and source current density, $\boldsymbol{\nu}$ and $\boldsymbol{\sigma}$ are the reluctivity and conductivity matrices given by

$$\boldsymbol{\nu}[i,j] = \int_\Omega \frac{1}{\mu} \boldsymbol{w}_i^2 \cdot \boldsymbol{w}_j^2 d\Omega, \quad \boldsymbol{\sigma}[i,j] = \int_\Omega \sigma \boldsymbol{w}_i^1 \cdot \boldsymbol{w}_j^1 d\Omega. \tag{5}$$

For the sake of brevity, the double curl operator in (3) will be denoted as $\boldsymbol{K} = \boldsymbol{C}^T \boldsymbol{\nu} \boldsymbol{C}$.

A. CLN as Material-Scale MOR

In a nutshell, the CLN method is about finding the equivalent circuit for the EC field, Fig. 1(b) [8]. The circuit parameters are the norms of electric, $\boldsymbol{e}_{2n}$, and magnetic modes, $\boldsymbol{a}_{2n+1}$ with weight functions $\boldsymbol{\sigma}$ and $\boldsymbol{K}$, respectively as

$$1/R_{2n} = \boldsymbol{e}_{2n}^T \boldsymbol{\sigma} \boldsymbol{e}_{2n}, \tag{6}$$
$$L_{2n+1} = \boldsymbol{a}_{2n+1}^T \boldsymbol{K} \boldsymbol{a}_{2n+1}. \tag{7}$$

Electric and magnetic modes hold the orthogonality and are obtained by the following recurrence formulae:

$$\boldsymbol{K}(\boldsymbol{a}_{2n+1} - \boldsymbol{a}_{2n-1}) = \frac{1}{R_{2n}} \boldsymbol{\sigma} \boldsymbol{e}_{2n}, \tag{8}$$
$$\boldsymbol{e}_{2n+2} - \boldsymbol{e}_{2n} = -\frac{1}{L_{2n+1}} \boldsymbol{a}_{2n+1}. \tag{9}$$

The CLN procedure initiates with a unit voltage source on the external excitation terminals, which sets up the first electric mode $\boldsymbol{e}_0$, and it continues as in Algorithm 1.

B. Laminated Core Homogenization as Material-Scale MOR

At the lamination scale, the magnetic flux distribution along the thickness direction of a steel sheet is described by Legendre polynomials $P_{2n}(-1 \leq x \leq 1, n = 0, 1, \cdots)$ as

$$B(t,z) = b_0(t) P_0\left(\frac{2z}{d}\right) + b_2(t) P_2\left(\frac{2z}{d}\right) + \cdots \tag{10}$$

where d and z are the lamination thickness and stacking direction, and $b_0, b_2, \cdots$ the homogenized components of induction [3]. Then the magnetic intensity on the surface of the lamination $H_s$expanded as

$$\begin{bmatrix} H_s(t) \\ 0 \\ \vdots \end{bmatrix} = \nu \begin{bmatrix} 1 & 0 & \cdots \\ 0 & \frac{1}{5} & \cdots \\ \vdots & \vdots & \ddots \end{bmatrix} \begin{bmatrix} b_0(t) \\ b_2(t) \\ \vdots \end{bmatrix} + \sigma d^2 \begin{bmatrix} \frac{1}{12} & \frac{-1}{60} & \cdots \\ \frac{-1}{60} & \frac{1}{210} & \cdots \\ \vdots & \vdots & \ddots \end{bmatrix} \frac{\mathrm{d}}{\mathrm{d}t} \begin{bmatrix} b_0(t) \\ b_2(t) \\ \vdots \end{bmatrix}. \tag{11}$$

Insulation layers are considered by increased reluctivity ν/α, and decreased conductivity $\alpha\sigma$, with α the fill factor of the laminated core $(0 < \alpha \leq 1)$.

While the EC in Fig. 1 (a-left) is governed by (3), the homogenized EC field in Fig. 1 (a-right) is obtained by integrating (11) into (3). On macroscopic scale, FE utilizes the magnetic field strength on the lamination surface and averaged flux density in stacking direction, which are equivalent to H_s and b_0 in (11), respectively. Homogenized EC equation over the entire domain Ω is a combination of (11) in the laminated region Ω_l (with $\boldsymbol{C}_l$ as edge-face incident matrix on Ω_l) with the standard constitutive laws in non-laminated regions:

$$\boldsymbol{K'}\underline{\boldsymbol{a}} = \boldsymbol{\sigma'} \partial_t \underline{\boldsymbol{a}} + \underline{\boldsymbol{j}_0}, \tag{12}$$

where

$$\boldsymbol{K'} = \begin{bmatrix} \boldsymbol{C}^T \boldsymbol{\nu} \boldsymbol{C} & 0 & \cdots \\ 0 & \boldsymbol{C}_l^T \frac{\boldsymbol{\nu}_l}{5} \boldsymbol{C}_l & \cdots \\ \vdots & \vdots & \ddots \end{bmatrix}, \tag{13}$$

$$\boldsymbol{\sigma'} = \begin{bmatrix} \boldsymbol{\sigma} + \boldsymbol{C}^T \frac{\boldsymbol{\sigma}_l d^2}{12} \boldsymbol{C} & -\boldsymbol{C}^T \frac{\boldsymbol{\sigma}_l d^2}{60} \boldsymbol{C}_l & \cdots \\ -\boldsymbol{C}_l^T \frac{\boldsymbol{\sigma}_l d^2}{60} \boldsymbol{C} & \boldsymbol{C}_l^T \frac{\boldsymbol{\sigma}_l d^2}{210} \boldsymbol{C}_l & \cdots \\ \vdots & \vdots & \ddots \end{bmatrix}, \tag{14}$$

$$\underline{\boldsymbol{a}} = [\boldsymbol{a}_0, \boldsymbol{a}_{2,l}, \cdots]^T, \quad \underline{\boldsymbol{j}_0} = [\boldsymbol{j}_0, 0, \cdots]^T. \tag{15}$$

where $\boldsymbol{\nu}_l$ and $\boldsymbol{\sigma}_l$ are the homogenized permeability and conductivity matrices in Ω_l given by

$$\boldsymbol{\nu}_l[i,j] = \int_{\Omega_l} \frac{1}{\alpha\mu} \boldsymbol{w}_i^2 \cdot \boldsymbol{w}_j^2 d\Omega, \quad \boldsymbol{\sigma}_l[i,j] = \int_{\Omega_l} \alpha\sigma \boldsymbol{w}_i^2 \cdot \boldsymbol{w}_j^2 d\Omega. \tag{16}$$

III. Derivation of Multi-Scale MOR

In this paper multi-scale MOR is about generating the equivalent Cauer ladder network for homogenized EC field in (12). Because the aforementioned homogenization [3] has a high compatibility with FE, generating the CLN process for that is straightforward and relatively similar to the

Algorithm 2 CLN Procedure on Hom. EC Field

$\underline{\boldsymbol{a}}_{-1} = 0$
$1/R_0 = \underline{\boldsymbol{e}}_0^T \boldsymbol{\sigma'} \underline{\boldsymbol{e}}_0$
for $n = 0$ **to** $n = \#stages$ **do**
  $solve : \boldsymbol{K'} \underline{\tilde{\boldsymbol{a}}}_{2n+1} = R_{2n} \boldsymbol{\sigma'} \underline{\boldsymbol{e}}_{2n}$
  $\underline{\boldsymbol{a}}_{2n+1} = \underline{\tilde{\boldsymbol{a}}}_{2n+1} + \underline{\boldsymbol{a}}_{2n-1}$
  $L_{2n+1} = \underline{\boldsymbol{a}}_{2n+1}^T \boldsymbol{K'} \underline{\boldsymbol{a}}_{2n+1}$
  $\underline{\boldsymbol{e}}_{2n+2} = \underline{\boldsymbol{e}}_{2n} - L_{2n+1}^{-1} \underline{\boldsymbol{a}}_{2n+1}$
  $1/R_{2n+2} = \underline{\boldsymbol{e}}_{2n+2}^T \boldsymbol{\sigma'} \underline{\boldsymbol{e}}_{2n+2}$
end for

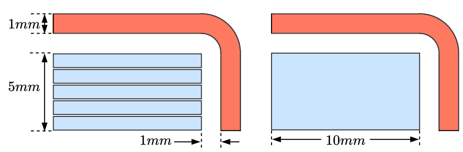

Fig. 2. One quarter of FE model -left: RM -right: homogenized.

standard procedure. The CLN procedure on homogenized EC is depicted in Algorithm 2.

The accuracy of the material-scale MOR is controlled by the number of homogenized components of induction (i.e. size of $\boldsymbol{K'}$ and $\boldsymbol{\sigma'}$). Additionally, the accuracy of machine-scale MOR is determined by number of CLN stages. As a rule of thumb, the optimum configuration of the proposed multi-scale MOR is obtained when the number of CLN stages is equal to the number of homogenized components of induction.

IV. Numerical Examples

Accuracy of the proposed multi-scale method is demonstrated by applying it to a 2-D laminated core, extended to infinity in z direction using FreeFEM++ software [12]. The core is wrapped by a cylindrical shaped coil carrying the external current density $\boldsymbol{j}_0$. The core is comprised of 2×5 laminations with $d = 0.5$mm, relative permeability $\mu_r = 2000$, conductivity $\sigma = 1$MS/m and fill factor $\alpha = 0.9$. The excitation coil width is 0.2mm with conductivity $\sigma = 40$MS/m. Due to the symmetry, only a quarter of the Reference Model (RM) is analyzed and shown in Fig. 2(left). Fig. 2(right) illustrates the geometry of the homogenized core using (13). Magnetic vector potential $\boldsymbol{A}$ and electric field $\boldsymbol{E}$ are approximated by in-plane shape function. Magnetic flux density $\boldsymbol{B}$, is perpendicular to the plane.

Conducting Algorithm 1 on RM gives the CLN parameters as a machine-scale MOR. On the other hand, proposed multi-scale MOR comes from applying Algorithm 2 on 0^{th} and 2^{nd} order homogenized fields. Those parameters are tabulated in Table 1 too.

Frequency responses are compared with the admittance per unit length seen by source by plotting $\mathrm{Re}(Y)$ and inductance $L = \mathrm{Im}(1/Y)/\omega$ in Fig 3 and Fig. 4. When the excitation coil is fed with a unit alternating voltage source with the angular velocity of ω, the admittance in RM and homogenized model

TABLE I
CLN Parameters Obtained for the Reference Model, 0^{th} and 2^{nd} Order Homogenized Model.

Ω/m	RM	0^{th}Hom.	2^{nd}Hom.	H/m	RM	0^{th}Hom.	2^{nd}Hom.
R_0	1.05e-06	1.05e-06	1.05e-06	L_1	2.83e-08	2.83e-08	2.83e-08
R_2	6.72e-04	6.67e-04	6.67e-04	L_3	5.31e-09	2.25e-12	5.65e-09
R_4	9.04e-04	4.70e-07	1.55e-03	L_5	2.09e-08	6.29e-08	2.18e-08
R_6	9.49e-07	3.54e-05	8.09e-07	L_8	4.58e-09	1.20e-10	2.21e-12

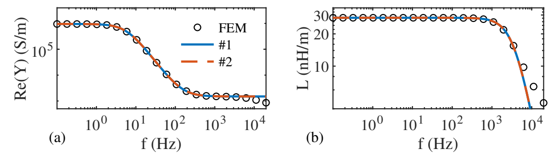

Fig. 3. Frequency responses obtained with RM, 0^{th} order Homogenization and it's equivalent CLN (#1: single stage CLN, #2: two stage CLN).

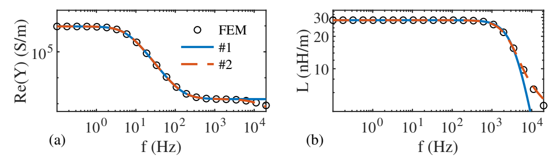

Fig. 4. Frequency responses obtained with RM, 2^{nd} order Homogenization and it's equivalent CLN (#1: single stage CLN, #2: two stage CLN).

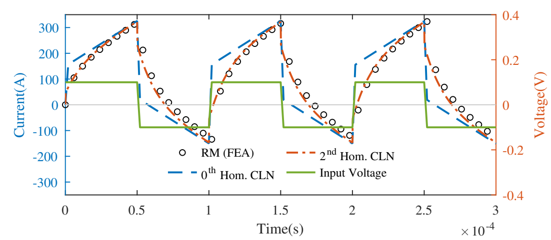

Fig. 5. Transient response to rectangular excitation.

are

$$Y_{\mathrm{RM}} = (\boldsymbol{e}_0 - j\omega \boldsymbol{a})^T \boldsymbol{\sigma} (\boldsymbol{e}_0 - j\omega \boldsymbol{a}) + j\omega \boldsymbol{a}^T \boldsymbol{K} \boldsymbol{a}, \quad (17)$$

$$Y_{\mathrm{H}} = (\underline{\boldsymbol{e}}_0 - j\omega \underline{\boldsymbol{a}})^T \boldsymbol{\sigma'} (\underline{\boldsymbol{e}}_0 - j\omega \underline{\boldsymbol{a}}) + j\omega \underline{\boldsymbol{a}}^T \boldsymbol{K'} \underline{\boldsymbol{a}}. \quad (18)$$

Transient analysis are carried out with square wave unit voltage excitation at 10kHz. Transient responses obtained from FE on RM and its zero and second order equivalent CLN are depicted in Fig. 5. It is simply obvious that the losses in the CLN resistances are equivalent to EC loss [8] in Fig. 6(a). The EC losses separated in coil and core regions are derived using energy division method in Appendix B and compared with FEA in Fig. 6(b-c). The reconstructed magnetic flux density fields on the center-line are shown in Fig. 7. The discrepancies are mainly due to the U-turns of the ECs at the far end side of the laminations which are basically neglected in the homogenization stage.

On Fig. 5, to obtain the RM results with 54540 number of unknowns, it took 1101s using on a computer with a clock frequency of 2.9 GHz and 16.0 GB of RAM. The computational time required to get 0^{th} and 2^{nd} order Hom. CLN results with 3148 and 4017 number of unknowns were 0.31s and 0.73s respectively.

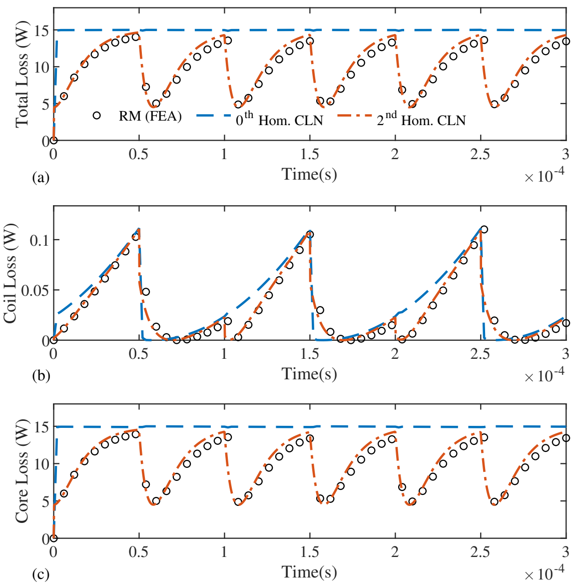

Fig. 6. EC losses on entire domain (a), coil (b) and core(c)

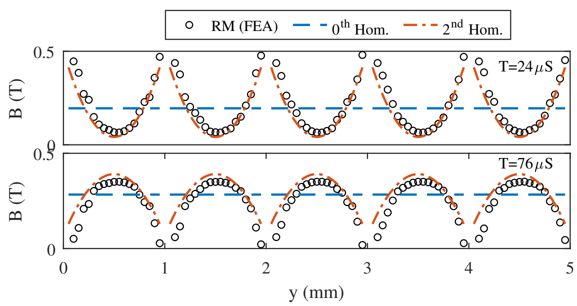

Fig. 7. The distribution of magnetic field at the center-line.

V. Conclusion

In this paper a multi-scale MOR method was presented as a combination of material-scale and machine-scale MORs. EC loss separation over arbitrary sub-domains was also developed as an useful feature of CLN method. Numerical examples showed that both frequency and transient responses agreed well with the FE on the reference model. The further steps to be taken are multi-port and nonlinear extensions of the presented work.

Appendix A

Due to the distributive property of integration, CLN parameters can be divided into arbitrary number of non-overlapping regions that fill the domain as a whole. For the sake of simplicity, we consider two complementary domains only; Ω_α and Ω_β. The CLN parameters in (6)-(7) are rewritten as:

$$\begin{aligned}\frac{1}{R_{2n}} &= \boldsymbol{e}_{2n}^T\boldsymbol{\sigma}\boldsymbol{e}_{2n} = \boldsymbol{e}_{2n}^T(\boldsymbol{\sigma}_\alpha + \boldsymbol{\sigma}_\beta)\boldsymbol{e}_{2n} \\ &= \frac{1}{R_{2n,\alpha}} + \frac{1}{R_{2n,\beta}}, \end{aligned} \tag{19}$$

$$\begin{aligned} L_{2n+1} &= \boldsymbol{a}_{2n+1}^T\boldsymbol{K}\boldsymbol{a}_{2n+1} = \boldsymbol{a}_{2n+1}^T(\boldsymbol{K}_\alpha + \boldsymbol{K}_\beta)\boldsymbol{a}_{2n+1} \\ &= L_{2n+1,\alpha} + L_{2n+1,\beta}, \end{aligned} \tag{20}$$

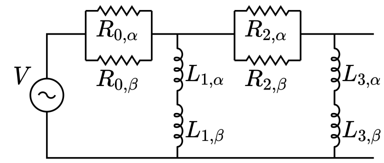

Fig. 8. CLN with divided parameters.

where

$$\begin{aligned} &\boldsymbol{K}_x = \boldsymbol{C}\boldsymbol{\nu}_x\boldsymbol{C}, (x = \alpha \text{ or } \beta) \\ &\boldsymbol{\nu}_x[i,j] = \int_{\Omega_x}\frac{1}{\mu}\boldsymbol{w}_i^2\cdot\boldsymbol{w}_j^2\mathrm{d}\Omega, \quad \boldsymbol{\sigma}_x[i,j] = \int_{\Omega_x}\sigma\boldsymbol{w}_i^1\cdot\boldsymbol{w}_j^1\mathrm{d}\Omega. \end{aligned} \tag{21}$$

This feature enables the calculation of the stored magnetic energy or loss dissipation at the desired domain, as shown in Fig. 8.

Acknowledgment

This work was supported in part by the Japan Society for the Promotion of Science under Grant-in-Aid for Scientific Research (C) No. 20K04443. H. Eskandari gratefully acknowledges financial and invaluable moral support from the Yoshida Scholarship Foundation.

References

[1] T. Henneron and S. Clénet, "Proper generalized decomposition method applied to solve 3-D magnetoquasi-static field problems coupling with external electric circuits," in IEEE Trans. on Magn., vol. 51, no. 6, pp. 1-10, June 2015, Art no. 7208910.

[2] Y. Sato et al., "Synthesis of Cauer-equivalent circuit based on model order reduction considering nonlinear magnetic property," in IEEE Trans. on Magn., vol. 53, no. 6, pp. 1-4, June 2017, Art no. 1100204.

[3] J. Gyselinck et al., "Finite-element homogenization of laminated iron cores with inclusion of net circulating currents due to imperfect insulation," IEEE Trans. on Magn., vol. 52, no. 3, pp. 1–4, 2016.

[4] K. Hollaus and M. Schöbinger, "A mixed multiscale FEM for the eddy-current problem with T, $\Phi - \Phi$ in laminated conducting media," in IEEE Trans. on Magn., vol. 56, no. 4, pp. 1-4, April 2020, Art no. 7515404.

[5] C. A. Valdivieso et al., "Time-domain finite-element eddy-current homogenization of windings using foster networks and recursive convolution," in IEEE Trans. on Magn., vol. 56, no. 12, pp. 1-8, Dec. 2020, Art no. 7401408.

[6] R. V. Sabariego and J. Gyselinck, "Time-domain reduced-order modelling of linear finite-element eddy-current problems via RL-ladder circuits," Scientific Computing in Electrical Engineering Mathematics in Industry, pp. 231–239, 2018.

[7] T. Matsuo et al., "Matrix formulation of the Cauer ladder network method for efficient eddy-current analysis," IEEE Trans. on Magn., vol. 54, no. 11, Art. No. 7205805, Nov. 2018.

[8] A. Kameari et al., "Cauer ladder network representation of eddy-current fields for model order reduction using finite-element method," IEEE Trans. on Magn., vol. 54, no. 3, Art. No. 7201804, Mar. 2018.

[9] T. Matsuo et. al., "Model order reduction of an induction motor using a Cauer ladder network," IEEE Trans. on Magn., vol. 56, no. 3, Art. No. 7514704, Jan. 2020.

[10] Y. Shindo et al., "Cauer circuit representation of the homogenized eddy-current field based on the Legendre expansion for a magnetic sheet," IEEE Trans. on Magn., vol. 52, no. 3, pp. 1–4, 2016.

[11] A. Bossavit, Computational Electromagnetism, San Diego, CA, USA:Academic Press, 1998.

[12] F. Hecht, "New development in FreeFem++", J. Numer. Math, vol. 20, no. 3-4, pp. 251-265, 2012.